Study of the electrochemical behaviour of SLM and traditional CoCrMo alloys in simulated body fluids

M. Seyedi[1], A. Balbo[2], F. Zanotto[3], E. Liverani[4], A. Fortunato[5], C. Monticelli[6]

[1] *Centro di Studi sulla Corrosione e Metallurgia "A. Dacco", Dipartimento di Ingegneria, Università degli Studi di Ferrara, via G. Saragat 4a, 44122 Ferrara ; Italy, mahla.seyedi@unife.it*

[2] *Centro di Studi sulla Corrosione e Metallurgia "A. Dacco", Dipartimento di Ingegneria, Università degli Studi di Ferrara, via G. Saragat 4a, 44122 Ferrara ; Italy, andrea.balbo@unife.it*

[3] *Centro di Studi sulla Corrosione e Metallurgia "A. Dacco", Dipartimento di Ingegneria, Università degli Studi di Ferrara, via G. Saragat 4a, 44122 Ferrara ; Italy, federica.zanotto@unife.it*

[4]*Dipartimento di Ingegneria Industriale, Università di Bologna, Bologna ; Italy, erica.liverani2@unibo.it*

[5]*Dipartimento di Ingegneria Industriale, Università di Bologna, Bologna ; Italy, alessandro.fortunato@unibo.it*

[6] *Centro di Studi sulla Corrosione e Metallurgia "A. Dacco", Dipartimento di Ingegneria, Università degli Studi di Ferrara, via G. Saragat 4a, 44122 Ferrara ; Italy, cecilia.monticelli@unife.it*

Abstract:
In this work, the electrochemical behaviour of the selective laser melting (SLM) CoCrMo alloy in simulated body fluid was investigated and compared with that of traditional CoCrMo alloy.
The microstructure of the studied samples was characterized by SEM/EDS and X-Ray Diffraction.
The electrochemical behaviour was investigated during immersion in phosphate buffer saline (PBS) solution at pH 7.4 and at pH 4 with and without the addition of H_2O_2 at the concentration of 30 mM, in order to simulate both normal and inflammatory conditions.
During the exposure to simulated body fluids, electrochemical impedance spectroscopy (EIS) and cyclic voltammetry tests were conducted to study the electrochemical behaviour of CoCrMo alloys.
The alloy manufactured with SLM technique showed a very fine and elongated cellular microstructure, characterized by enrichment in Mo at the cell boundaries and suppressed carbide precipitation. Both the SLM and traditional alloys showed low corrosion rates in the studied environments because of the formation of a very protective oxide film on the sample surfaces with high resistance to localized corrosion, but the traditional alloy exhibited the lowest corrosion rates.
A comparison of cyclic voltammetry tests carried out on SLM and traditional CoCrMo alloys revealed that, even if the alloys are passive in all PBS solutions, the passive film in the presence of inflammatory species is not as protective as that formed under normal physiological conditions. The CV results showed that the elemental Co, Cr and Mo react with the electrolyte medium and the passive film is mainly composed of Cr_2O_3 with some amounts of Co(II) hydroxide (only at pH 7.4), MoO_2 and likely Mo complex oxides.

Keywords: Biomaterials, Selective laser melting, CoCrMo endoprosthesis, Simulated body fluids, Elechtrochemical behaviour.

Introduction

Biocompatible materials are generally used to replace hard tissues in orthopaedic or orthodontia which are damaged by severe trauma or to support damaged biological tissues, e.g. blood vessel stents or artificial valves in the heart [1,2].
CoCrMo alloys are widely used as biomaterials for orthopaedic implants, especially in artificial hip and knee joints, as well as dental prosthesis, due to their advanced ability to resist wear and corrosion, adequate mechanical properties and high biocompatibility compared to the other biomaterial alloys [3–6]. In the past decades, CoCrMo based implants were manufactured using traditional casting techniques. Although they featured to be used successfully as biomaterials for many years, in some cases clinical orthopaedic studies revealed implant failures [7]. The causes of these failures are ascribed to: limited availability of prosthesis sizes and shapes, differences in mechanical properties between bone and implant materials, unsatisfactory osteointegration and foreign body reactions induced by inflammatory cells [7–9]. The advancement of additive manufacturing technologies, such as selective laser melting (SLM), allowed to overcome some of these problems. This technique allows to obtain completely customizable prostheses with complex shapes by the consolidation of metal powders layer by layer through two main paths using the computer-aided design (CAD) and laser manufacturing process [10]. The precise control offered by SLM over microstructural characteristics of the product as well as the manufacturing of dense or porous graded components open the door to a single-step manufacturing process for highly customizable architectures, improving osteointegration and bone adaptation. The SLM manufacturing process imposes very high heating and cooling rates inducing non-equilibrium microstructural characteristics, not found in traditional materials [11–14]. The extent and success of osteointegration depend on the biocompatibility of the implanted material and the corrosion resistance of metal implants in the body fluids [15,16]. Selective laser melting is one of the recent promising processes for implant fabrication [13,17–20]. Although this technique allows to produce CoCrMo alloys with high corrosion resistance, their behaviour in biological environments need to be further investigated.
In the present work, the suitability of SLM CoCrMo alloys as implanted materials was assessed by focussing on their electrochemical behaviour in simulated body fluids (SBF). The electrochemical characterization was carried out by electrochemical impedance spectroscopy (EIS) and cyclic voltammetry (CV) tests, while the microstructural characterization was performed by means of scanning electron microscopy (SEM) and X-ray diffraction (XRD).
The electrochemical behaviour of SLM alloys was compared with that of traditional alloy.

Experimental

Materials

The SLM specimens were produced by a SISMA MYSINT100 system (Sisma, Piovene Rocchette, Italy) by using the laser parameters showed in table 1. The nominal composition of the CoCrMo commercial powder (LPW Technology Ltd, Runcorn Cheshire, UK) used in the SLM process are reported in table 2 and are in agreement with the ASTM F1537 standard. The hatch distance (space between two adjacent laser tracks) was maintained constant to the value of 0.06 mm and a chessboard laser scan strategy was adopted. The specimens of traditional alloy were obtained from a hot worked and heat treated rods (35 mm in diameter). The nominal composition of this alloy meets the ISO 5832-12 standard and corresponds to Co-28Cr 6Mo (see table 3).
The electrodes for electrochemical test were soldered to sheathed copper wires and then embedded in epoxy. Before the tests in SBFs, the exposed surfaces (about 1 cm^2 for SLM and

2 cm^2 for the traditional alloy) were ground with emery papers up to P2500 grade and polished to 1 μm with diamond suspension. Finally, the samples surfaces were washed thoroughly with distilled water, cleaned in ethanol inside an ultrasonic bath and dried with hot air.

Microstructural characterization

All materials were characterized by a Scanning Electron Microscope (SEM, Zeiss MA15/LaB6) coupled with an energy dispersive spectroscopy (EDS) system (X-Act/INCA, Oxford Instruments) and by X ray diffraction technique (Bruker D8 advances Billerica USA).

Environment and Electrochemical tests

The biological environment related to normal physiological conditions was reproduced by using a phosphate buffered saline (PBS) solution at pH=7.4, with the composition reported in table 4. In order to simulate the inflammatory conditions, a PBS solution at pH=4 was used, while more severe inflammation was reproduced by addition of 30 mM H_2O_2 to the acidic PBS solution. All used chemicals were of analytical grade, and demineralised grade water was employed in solution preparation. During the tests, the SBF temperature was maintained at 37°C.

Tab. 1 - Process parameters used for fabrication of SLM specimens

Sample	Power (W)	Scan speed (mm/s)	Fluence (J/mm3)
SLM	150	900	138.8

Tab. 2 - EDS chemical composition (wt%) of CoCrMo powders

(wt%)	C	N	Al	Si	Cr	Mn	Fe	Co	Ni	Mo	La
Average	≤ 0.04	0.09	0.05	0.77	28.06	0.68	0.12	64.23	nd	5.92	0.07
Std Dev.	/	0.06	0.05	0.05	0.33	0.1	0.04	0.16	/	0.11	0.03

Tab. 3 – Chemical composition (wt%) of traditional CoCrMo alloy

(wt%)	C	N	Al	Si	Cr	Mn	Fe	Co	Ni	Mo	La	P	S	W
Average	0.048	0.162	0.01	0.76	27.8	0.75	0.13	Bal.	0.066	5.43	0.07	0.005	0.0005	0.02

Table 4: Composition of simulated body fluids (SBF)

	PBS (pH=7.4)	PBS (pH=4)
Na_2HPO_4 (g/L)	1.42	1.42
KH_2PO_4 (g/L)	0.245	0.245
KCl (g/L)	0.2	0.18
NaCl (g/L)	8.8	8.32
Total Cl^- (M)	0.15	0.15
Λ (mS/cm)	17.15	16.56

Two different electrochemical tests were conducted: Electrochemical Impedance Spectroscopy (EIS) and Cyclic Voltammetry (CV) tests. The electrochemical tests were performed with a PAR 2263 potentiostat/FRA/ galvanostat (EIS), and with a PAR 273A potentiostat/galvanostat (CV).
The measurements were carried out in the conventional three-electrodes cell. The reference and auxiliary electrodes were a saturated calomel electrode (SCE) and a Pt sheet, respectively. All the potential values quoted in the text are referred to SCE.
The evolution of corrosion behaviour was monitored by recording the EIS spectra during 15 days of exposure to SBFs at 37°C. The EIS spectra were collected at the corrosion potential (E_{cor}) by imposing a 10 mV(rms) amplitude excitation voltage in the 10^4 –10^{-3} Hz frequency range, and by acquiring 10 measurements per decade. From each spectrum the polarization resistance (R_p) value was estimated as the limit of the real part of the impedance at frequency tending to 0.
Cyclic voltammetry tests were performed in order to investigate the contribution of the different alloying elements to the electrochemical behaviour of the 2 alloys. The cyclic voltammograms were recorded at a scan rate of 120 mV/s, under constant stirring conditions. Before the test, the samples were polarized at -1.5 V(SCE) for 80 s.

Results and discussion

Figure 1 shows the microstructures of SLM and traditional samples obtained after electrolytic etching. The high fluence of the SLM processes induced powder melting and allowed to obtain high relative density (99.85 %). During the SLM process, under a high-energy laser beam, the alloy underwent a rapid melting followed by a rapid cooling that produced an undercooled melt. The high solidification rates and the high level of non-equilibrium conditions suppressed the formation of micro-sized carbides and produced a fine and elongated cellular microstructure (figure 1A, cell size in the range 1000-450nm) formed within the melt pool. The traditional CoCrMo sample, obtained from a hot worked and heat treated rod, exhibited a microstructure (figure 1B) coarser than that of SLM alloy with equiaxed grains (grain size about 8µm) and strain-induced twins.

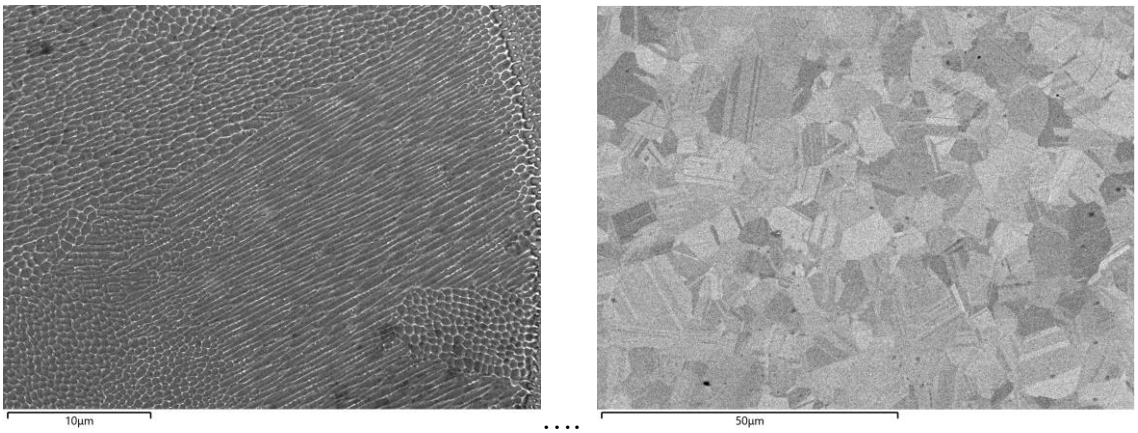

A B

Figure 1: SEM image of etched sample surfaces: SLM CoCrMo (A) and Traditional CoCrMo (B) cellar microstructure.

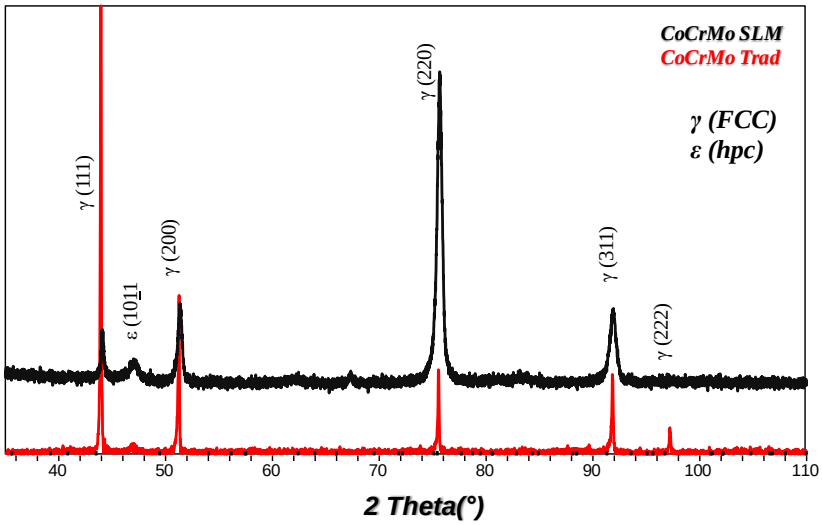

Figure 2: XRD diffraction pattern of SLM and traditional specimens.

The XRD diffraction patterns of the two alloys, obtained under spinning conditions, are shown in figure 2. The metastable fcc phase (γ phase) is the main phase in both alloys. However, some amounts of ε phase were detected especially in SLM samples (figure 2, peak at 46.5°) probably because of the γ→ ε transformation induced in the underlying layers during each new layer building up. The XRD pattern of SLM samples showed a low intensity for the (111) peak compared with the (200) and (220) peaks suggesting a texturing effect due to SLM process. The larger FWHM (full width at half maximum) of SLM peaks compared to that of the traditional sample suggested a lower crystallite size for the former alloy.

The corrosion behaviour of the two samples was studied by monitoring the polarization resistance (R_p) and corrosion potential (E_{corr}) during 15 days of exposure to the selected SBFs and the collected data are reported in tables 5 and 6, respectively.

Table 5: R_p values recorded during 15 days of exposure to SBFs

R_p (Ohm. cm^2)	**SLM**			**Traditional**		
	pH = 7.4	***pH = 4***	***pH =4+ 30 mM H_2O_2***	***pH = 7.4***	***pH = 4***	***pH =4+ 30 mM H_2O_2***
1h	2.08×10^5	5.46×10^5	1.81×10^5	6.67×10^5	3.14×10^6	5.49×10^5
1 day	4.17×10^6	3.36×10^6	4.84×10^5	4.41×10^6	5.08×10^6	3.25×10^6
5 days	8.57×10^6	5.50×10^6	2.29×10^6	8.30×10^6	1.07×10^7	3.78×10^6
10 days	1.03×10^7	7.17×10^6	2.24×10^6	1.31×10^7	1.58×10^7	2.70×10^6
15 days	9.04×10^6	2.03×10^6	1.66×10^6	1.77×10^7	1.78×10^7	2.56×10^6

Table 6: E_{corr} values documented during 15 days of immersion in SBFs

E_{corr} V/SCE	SLM			Traditional		
	pH = 7.4	**pH = 4**	**pH = 4 + 30 mM H_2O_2**	**pH = 7.4**	**pH = 4**	**pH = 4 + 30 mM H_2O_2**
1 hour	-0.275	-0.256	-0.0310	-0.295	-0.295	-0.038
1 day	-0.230	-0.136	0.176	-0.193	-0.198	0.390
5 days	-0.143	-0.058	0.274	-0.139	0.012	0.394
10 days	-0.137	-0.025	0.242	-0.136	0.043	0.382
15 days	-0.137	-0.027	0.231	-0.133	0.085	0.355

After 1 h immersion in PBS at pH= 7.4, the SLM sample showed R_p values of 0.2 MΩ cm^2 which is around three times lower than that of traditional one (~0.7 MΩ cm^2). During the first 5 days of immersion, R_p increased rapidly up to 0.8 MΩ cm^2 for both samples and then, the traditional alloy maintained only slightly higher R_p values (1.7 MΩ cm^2) than SLM (0.9 MΩ cm^2), until the end of the immersion period.

The corresponding E_{cor} values (table 6) increased during the first days of exposure on both samples and then, in the case of SLM sample, they settled at about -0.140 V_{SCE}, until the end of the exposure.

The R_p values measured at pH=4 (in the absence of H_2O_2) showed trends similar to those recorded at pH = 7.4. However, while the SLM sample exhibited R_p values always lower than those measured at pH = 7.4, on traditional alloy, these values were always slightly higher than that recorded in neutral PBS solution. At pH = 4 the E_{cor} values measured on both alloys showed a rapid ennobling after the first days of immersion and settled around -0.03V in the case of the SLM sample, while a slight constant increase up to 0.085V was measured on the traditional alloy.

The presence of H_2O_2 induced higher E_{cor} values than those recorded at the same pH but in the absence of this compound and reduced the corrosion resistance of both alloys. In fact, at the end of the exposure in this environment, R_p values of about 1.6 MOhm and a 2.6 MOhm were measured for SLM and traditional alloys, respectively. As far as the traditional alloy is concerned, the values measured in the presence of H_2O_2 were approximately one order of magnitude lower than those measured at pH = 4, but still higher than those measured on the SLM alloy in the same environment (pH = 4 + 30Mmol H_2O_2).

These results indicated an increase in corrosion resistance of both alloys during the exposure in the selected SBFs. The concurrent R_p increase and E_{cor} ennobling suggested that air-formed oxide films of improved protectiveness formed, due to an increase in thickness or defect concentration.

The decrease in solution pH slightly impaired the corrosion resistance of SLM samples, while in the case of the traditional alloy it did not affect the protective properties of the passive film. In the presence of H_2O_2 the passive film formed on the samples surface was, probably, thinner and more defective than that formed in absence of H_2O_2, and induced a decrease in corrosion resistance of both alloys. The traditional alloy still showed a better corrosion behaviour.

Cyclic voltammetry was used to gain further understanding of the mechanisms involved in the passive film formation and on its stability in the different environments. The results of CV tests were shown in figure 3, where the first and last voltammetry cycles collected on SLM and traditional alloy are compared. In all environments, three possible regions can be observed in the potential range examined: the hydrogen evolution region, the passive region and the transpassive region. The passive region is related to the formation of Cr_2O_3 oxide, generally in

the potential range between -1 V_{SCE} and +0.4-0.5 V_{SCE}, while at higher potentials the transpassive region occurs, related to the formation of soluble CrO_4^{2-} and MoO_4^{2-} species, beside oxygen evolution.

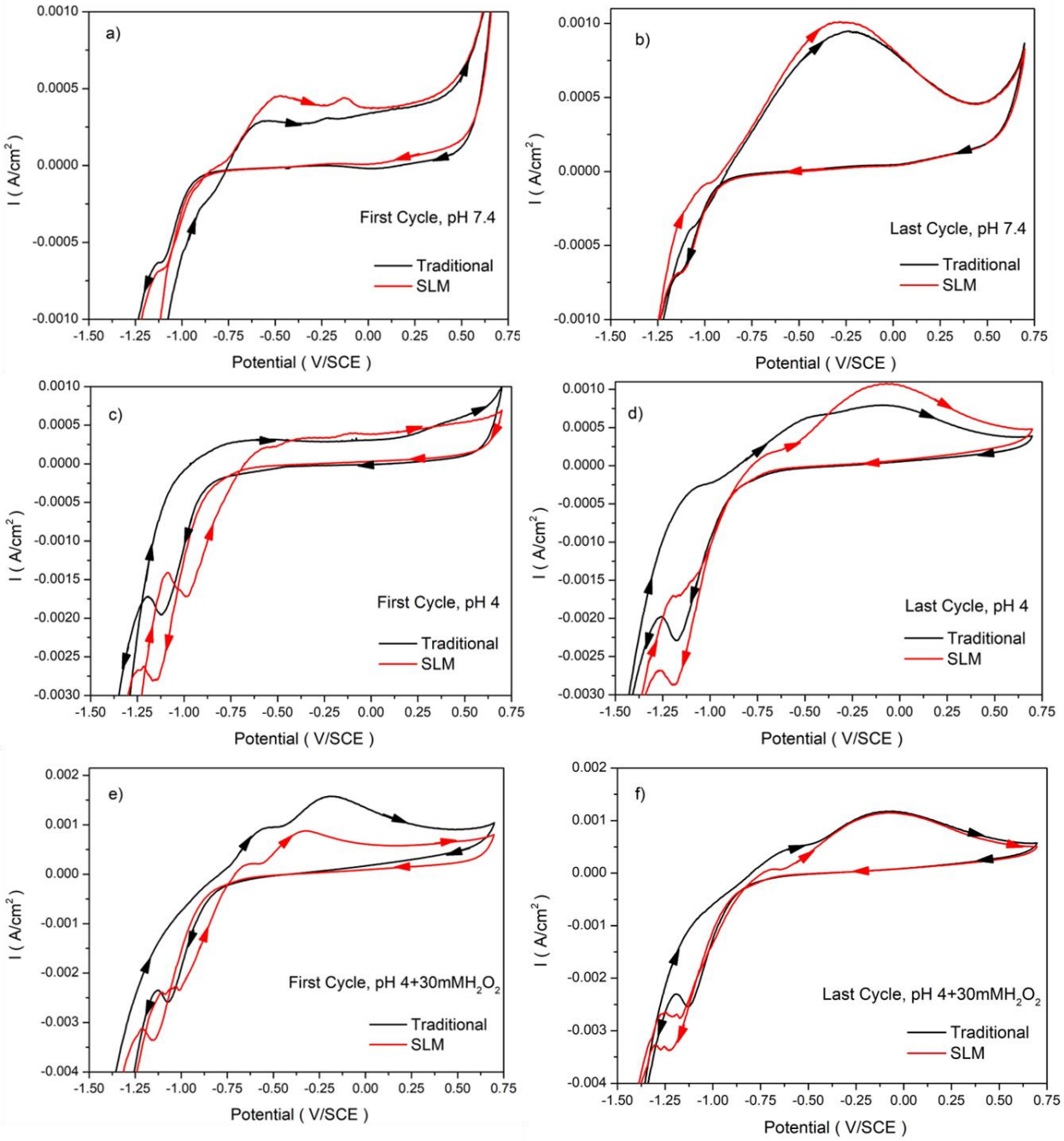

Fig. 3. Cyclic voltammograms recorded on SLM and traditional samples in different simulated body fluids: PBS pH=7.4 (a and b), PBS pH=4 (c and d) and PBS pH=4+30 mM H_2O_2 (e and f)

In the first cycle, on both materials, two anodic current peaks are observed at pH=7.4 (Fig.3a). The first broad current peak with a maximum at -0.50 V_{SCE} was related to the MoO_2 formation and to the oxidation of cobalt to Co(II) hydroxide likely favoured by a pre-existing of Cr_2O_3 layer not completely reduced during the cathodic pre-treatment [21]. Instead,, the peak at -0.1 V_{SCE} could be associated to the formation of a molybdenum complex oxide ($MoO_2 \cdot MoO_3$) [22]. The large anodic peak (fig 3b) recorded in the last cycle represents the combined oxidation of cobalt to Co(II) hydroxide on Cr_2O_3 layer and Mo oxidation to MoO_2 and complex Mo oxides. The slightly lower anodic peaks observed on the traditional alloy suggested a corresponding slightly higher oxidation resistance. At pH=4, in the first cycle (Fig. 4c), the peaks were less evident than those recorded at neutral pH, and the anodic current was mainly associated to the formation of Cr_2O_3. In the last cycle (Fig. 4d), on the traditional alloy, again two peaks were detected related to the formation of Mo_2O and a Mo-complex oxide, while on SLM alloy only one large peak centred at around -0.05V occurred, which was assigned to the probable formation of Mo oxides.
At pH = 4 in the presence of H_2O_2 (Fig. 3e and f), besides the formation of Cr_2O_3, two main peaks were still observed and were again correlated to the formation of MoO_2 and $MoO_2.MoO_3$, on both alloys. In this environment, higher oxidation peaks than those measured in the other SBFs were always measured, indicating a higher instability of the surface film. This was confirmed by the shift of the oxidation peaks towards more negative values and the reduction peaks towards less negative values, suggesting a higher reaction reversibility. These results suggested that the passive film formed in the presence of H_2O_2 was more defective and less protective than that formed at pH neutral or at pH 4 (with no additive), leading to higher oxidation rates, in accordance with the data obtained from EIS measurements.

Conclusion

Cyclic voltammetry and electrochemical impedance spectroscopy were used to study the passivation and corrosion behaviours of SLM and traditional CoCrMo alloys in simulated body fluids and at different pH values.
The studied materials showed low corrosion rates in the tested environment that decreased during the exposure. However, the traditional alloy exhibited the best performances. In the presence of H_2O_2 at pH=4, higher corrosion rates were detected on both alloys, because of a higher instability of the passive films.
The corrosion resistance of these alloys was related to the presence of a Cr_2O_3 film also containing Co(II) hydroxide (at pH 7.4), MoO_2 and Mo complex oxides.

References

[1] D.F. Williams, Implantable prostheses, Phys. Med. Biol. 25 (1980) 611–636.
[2] A.C. Hänzi, I. Gerber, M. Schinhammer, J.F. Löffler, P.J. Uggowitzer, Acta Biomater. 6 (2010) 1824–1833.
[3] M.M. Dewidar, H.C. Yoon, J.K. Lim, Met. Mater. Int. 12 (2006) 193–206.
[4] D. Williams, Biocompatibility of Clinical Implant Mtls, (1981).
[5] F. Contu, B. Elsener, H. Böhni, J. Electrochem. Soc. 150 (2003) B419.
[6] A. Marti, Injury. 31 (2000) D18–D21.
[7] N. Gougoulias, A. Khanna, N. Maffulli, Clin. Orthop. Relat. Res. 468 (2010) 199–208.
[8] S. Sivan, Y. Liu, S.B. Kocagöz, C.M. Arnholt, J.L. Gilbert, S.M. Kurtz, 103 (2014) 211–223.
[9] J.M. Anderson, A. Rodriguez, D.T. Chang, Semin. Immunol. 20 (2008) 86–100.
[10] S.L. Sing, Z.H. Liu, C.K. Chua, Z.L. Dong, D.Q. Zhang, C.Y. Yap, L.E. Loh, Appl. Phys. Rev. 2 (2015) 041101.

[11] X. zhen Xin, J. Chen, N. Xiang, B. Wei, Cell Biochem. Biophys. 67 (2013) 983–990.
[12] Y.S. Hedberg, B. Qian, Z. Shen, S. Virtanen, I. Odnevall Wallinder, Dent. Mater. 30 (2014) 525–534.
[13] S. Guo, Y. Gan, J. Lin, S. Zhang, J. Lin, Y. Lu, S. Wu, J. Mech. Behav. Biomed. Mater. 55 (2015) 179–190.
[14] S. Bose, S.F. Robertson, A. Bandyopadhyay, Acta Biomater. 66 (2018) 6–22.
[15] Q. Chen, G.A. Thouas, Mater. Sci. Eng. R Reports. 87 (2015) 1–57.
[16] D.F. Williams, Biomaterials. 29 (2008) 2941–2953.
[17] Y.S. Hedberg, B. Qian, Z. Shen, S. Virtanen, I. Odnevall Wallinder, Dent. Mater. 30 (2014) 525–534.
[18] Y. Lu, S. Wu, Y. Gan, T. Huang, C. Yang, L. Junjie, J. Lin, Opt. Laser Technol. 75 (2015) 197–206.
[19] M. Seyedi, F. Zanotto, C. Monticelli, A. Balbo, E. Liverani, A. Fortunato, Metall. Ital. (2018).
[20] E. Liverani, A. Fortunato, A. Leardini, C. Belvedere, S. Siegler, L. Ceschini, A. Ascari, (SLM), Mater. Des. 106 (2016) 60–68.
[21] M. Metikoš-Huković, Z. Pilić, R. Babić, D. Omanović, Acta Biomater. 2 (2006) 693–700.
[22] M.N. Hull, J. Electroanal. Chem. Interfacial Electrochem. 38 (1972) 143–157.